Three-Dimensional Color Code Thresholds via Statistical-Mechanical Mapping

Aleksander Kubica,[1,2,3] Michael E. Beverland,[1,4] Fernando Brandão,[4,1] John Preskill,[1] and Krysta M. Svore[4]
[1]*Institute for Quantum Information and Matter, California Institute of Technology, Pasadena, California 91125, USA*
[2]*Perimeter Institute for Theoretical Physics, Waterloo, Ontario N2L 2Y5, Canada*
[3]*Institute for Quantum Computing, University of Waterloo, Waterloo, Ontario N2L 3G1, Canada*
[4]*Station Q Quantum Architectures and Computation Group, Microsoft Research, Redmond, Washington 98052, USA*

(Received 30 September 2017; published 4 May 2018)

Three-dimensional (3D) color codes have advantages for fault-tolerant quantum computing, such as protected quantum gates with relatively low overhead and robustness against imperfect measurement of error syndromes. Here we investigate the storage threshold error rates for bit-flip and phase-flip noise in the 3D color code (3DCC) on the body-centered cubic lattice, assuming perfect syndrome measurements. In particular, by exploiting a connection between error correction and statistical mechanics, we estimate the threshold for 1D stringlike and 2D sheetlike logical operators to be $p^{(1)}_{\mathrm{3DCC}} \simeq 1.9\%$ and $p^{(2)}_{\mathrm{3DCC}} \simeq 27.6\%$. We obtain these results by using parallel tempering Monte Carlo simulations to study the disorder-temperature phase diagrams of two new 3D statistical-mechanical models: the four- and six-body random coupling Ising models.

DOI: 10.1103/PhysRevLett.120.180501

The two-dimensional (2D) surface code approach [1–3] to building scalable quantum computers has desirable features: (1) geometrically local syndrome measurements, (2) a high accuracy threshold, and (3) fault-tolerant Clifford gates with low overhead. Unfortunately, the surface code is *not* known to admit a (4) fault-tolerant non-Clifford gate with low overhead. The formidable qubit overhead of state distillation [4,5] for the necessary non-Clifford gate motivates the quest for alternatives to the surface code with all features 1–4.

Such alternatives may be sought in the general class of topological codes [1,2,6–8], which includes the surface code as a special case. By definition, topological codes require only geometrically local syndrome measurements and tend to have high accuracy thresholds. Topological codes often admit some fault-tolerant transversal gates (implemented by the tensor product of single-qubit unitaries), which have low overhead. However, no quantum error-detecting code (whether topological or not) has a universal transversal encoded gate set [9,10].

Here we focus on the 3D topological color codes [11,12] closely related to the 3D toric code [13], which come in two types. The stabilizer type has 1D stringlike Z and 2D sheetlike X logical operators, and a logical non-Clifford gate $T = \mathrm{diag}(1, e^{i\pi/4})$ is transversal. In the subsystem type, there are 1D stringlike X and Z dressed logical operators, and all logical Clifford gates are transversal. Moreover, in the subsystem color code, it is possible to reliably detect measurement errors in a single time step [14,15]. By fault-tolerantly switching between the stabilizer and subsystem color codes [12,16], one can combine the desirable features 1, 3, and 4.

In this Letter, we address feature 2 for the 3D color codes (3DCCs) by finding thresholds $p^{(1)}_{\mathrm{3DCC}} \simeq 1.9\%$ and $p^{(2)}_{\mathrm{3DCC}} \simeq 27.6\%$ for phase-flip Z and bit-flip X noise, respectively. Our results assume optimal decoders for independent X and Z noise with perfect measurements and thereby give fundamental error-correction bounds against which any decoder can be benchmarked [15,17,18]. These thresholds are comparable to the analogous thresholds for the cubic lattice 3D toric code (3DTC): $p^{(1)}_{\mathrm{3DTC}} \simeq 3.3\%$ and $p^{(2)}_{\mathrm{3DTC}} \simeq 23.5\%$ [19–21], but compare unfavorably to $p_{\mathrm{2DTC}} \simeq 10.9\%$ for the square lattice 2D toric code [22].

Our approach extends techniques known for other codes [3,8,23–28] in order to relate the 3D color code thresholds to phase transitions in two new 3D statistical-mechanical models: the four- and six-body random coupling Ising models (RCIMs). We use large-scale parallel tempering Monte Carlo simulations [29] and analyze specific heat, sublattice magnetization, and Wilson loop operators to map the relevant parts of the disorder-temperature (p, T)-phase diagram; see Fig. 1. The six-body RCIM is an example of a lattice gauge theory with a local (gauge) $\mathbb{Z}_2 \times \mathbb{Z}_2$ symmetry, which makes this model both interesting and numerically challenging to study.

Three-dimensional stabilizer color code.—Let $\mathcal{L}$ be a three-dimensional lattice built of tetrahedra such that its vertices are four colorable; i.e., vertices connected by an edge are differently colored. An example of such a lattice is the body-centered cubic (bcc) lattice obtained from two interleaved cubic lattices; see Fig. 2(b). We denote by $\Delta_i(\mathcal{L})$ the set of all i-simplices of $\mathcal{L}$. Then, zero-simplices of $\mathcal{L}$ are vertices, one-simplices are edges, etc. We place

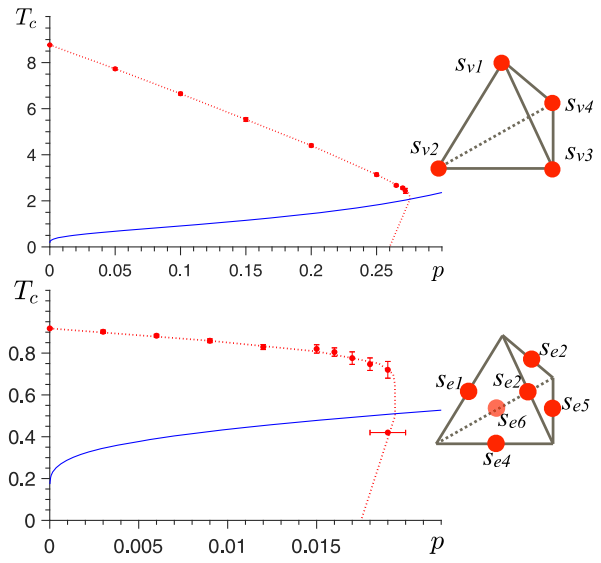

FIG. 1. The disorder-temperature (p, T)-phase diagrams of the four-body (top) and six-body (bottom) 3D random coupling Ising models defined on the 3D body-centered cubic lattice built of tetrahedra. The four- and six-body models have spins on vertices and edges, respectively. The storage threshold p_c can be found as the intersection of the Nishimori line (blue line) with the anticipated phase boundary (red dotted line).

one qubit at every tetrahedron $t \in \Delta_3(\mathcal{L})$. For every vertex $v \in \Delta_0(\mathcal{L})$ and edge $e \in \Delta_1(\mathcal{L})$, we define operators $S_X(v)$ and $S_Z(e)$ to be the product of either Pauli X or Z operators on qubits identified with tetrahedra in the neighborhood of the vertex v or edge e, namely,

$$S_X(v) = \prod_{\substack{t \in \Delta_3(\mathcal{L}) \\ t \supset v}} X(t), \qquad S_Z(e) = \prod_{\substack{t \in \Delta_3(\mathcal{L}) \\ t \supset e}} Z(t). \tag{1}$$

The 3D stabilizer [30] color code is defined by specifying its stabilizer group [31]

$$\mathcal{S} = \langle S_X(v), S_Z(e) | v \in \Delta_0(\mathcal{L}), e \in \Delta_1(\mathcal{L}) \rangle. \tag{2}$$

Using the colorability condition, one can show that $\mathcal{S}$ is an Abelian subgroup of the Pauli group not containing $-I$. The code space is the $+1$ eigenspace of all elements of $\mathcal{S}$ and the lowest-weight logical X and Z operators of the 3D color code are 2D sheetlike and 1D stringlike objects; see Fig. 2(a). In general, the color code can be defined in $d \geq 2$ dimensions on a lattice, provided it is a $(d+1)$-colorable simplicial d-complex [16].

Error correction in CSS codes.—Since the color code is a CSS code [32], we choose to separately correct X- and Z-type errors, which simplifies the discussion. We also assume perfect measurements. For concreteness, we focus on X error correction; Z errors can be analyzed analogously [33].

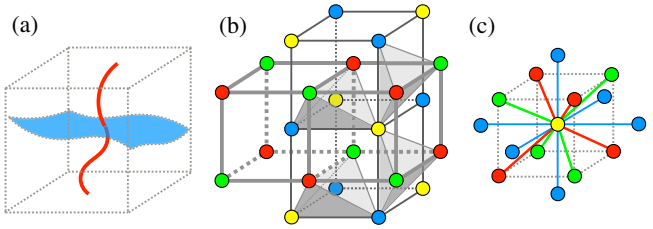

FIG. 2. (a) The 3D stabilizer color code has both 1D stringlike (red) and 2D sheetlike (blue) logical operators. (b) The bcc lattice is constructed from two interleaved cubic lattices by filling in tetrahedra (gray). Not all tetrahedra are depicted. (c) The neighborhood of any vertex in the bcc lattice looks the same—every vertex belongs to 24 edges, 36 triangular faces, and 24 tetrahedra. The bcc lattice is four colorable; i.e., every vertex is colored in red, green, blue, or yellow, and neighboring vertices are colored differently.

The set of all Z-type stabilizers which return -1 measurement outcomes is called a Z-type syndrome. Note that any nontrivial Z syndrome signals the presence of some X errors in the system. Correction of X errors in a CSS code is described by introducing a chain complex [17,34]

$$\underset{X \text{ stabilizers}}{C_2} \xrightarrow{\partial_2} \underset{\text{qubits}}{C_1} \xrightarrow{\partial_1} \underset{Z \text{ stabilizers}}{C_0} \tag{3}$$

where C_2, C_1, and C_0 are vector spaces over $\mathbb{Z}_2$ with bases $\mathcal{B}_2 = X$ stabilizer generators, $\mathcal{B}_1 =$ physical qubits, and $\mathcal{B}_0 = Z$ stabilizer generators, respectively. The linear maps ∂_2 and ∂_1, called boundary operators, are chosen in such a way that the support of any X stabilizer $\omega \in C_2$ is given by $\partial_2 \omega$, and the Z syndrome corresponding to any X error $\epsilon \in C_1$ can be found as $\partial_1 \epsilon$. Note that $\partial_1 \circ \partial_2 = 0$, since any X stabilizer has trivial Z syndrome. One can think of the boundary operators as parity-check matrices H_X^T and H_Z of the CSS code. In the case of the 3D color code, C_2, C_1, and C_0 are generated by vertices, tetrahedra, and edges, respectively; i.e., $\mathcal{B}_2 = \Delta_0(\mathcal{L})$, $\mathcal{B}_1 = \Delta_3(\mathcal{L})$, and $\mathcal{B}_0 = \Delta_1(\mathcal{L})$. The boundary operators are defined to be $\partial_2 v = \sum_{\Delta_3(\mathcal{L}) \ni t \supset v} t$ and $\partial_1 t = \sum_{\Delta_1(\mathcal{L}) \ni e \subset t} e$ for any $v \in \Delta_0(\mathcal{L})$ and $t \in \Delta_3(\mathcal{L})$.

Let $\epsilon, \varphi \in C_1$ be two X errors with the same Z syndrome, $\partial_1 \epsilon = \partial_1 \varphi$. We say that ϵ and φ are equivalent if and only if they differ by some X stabilizer $\omega \in C_2$, namely, $\epsilon + \varphi = \partial_2 \omega$. To correct errors, we need a decoder—an algorithm that takes the Z syndrome $\sigma \in C_0$ as an input and returns a Z correction φ restoring all X stabilizers to $+1$ outcomes; i.e., $\partial_1 \varphi = \sigma$. The decoder succeeds if and only if the actual error ϵ and the correction φ are equivalent. An optimal decoder finds a representative φ of the most probable equivalence class of errors $\bar{\varphi} = \{\varphi + \partial_2 \omega | \forall \omega \in C_2\}$.

Statistical-mechanical models.—In this section, we provide a brief derivation of the connection between optimal

error-correction thresholds and phase transitions [3,8,23–28]. In particular, we derive two new statistical-mechanical models relevant for the 3D color code.

We assume bit-flip noise; i.e., every qubit is independently affected by Pauli X error with probability p. The probability of an X error $\epsilon \in C_1$ affecting the system is

$$\mathrm{pr}(\epsilon) = \prod_{j\in\mathcal{B}_1} p^{[\epsilon]_j}(1-p)^{1-[\epsilon]_j} \propto \left(\frac{p}{1-p}\right)^{\sum_{j\in\mathcal{B}_1}[\epsilon]_j}, \quad (4)$$

where $[\epsilon]_j \in \mathbb{Z}_2$ denotes the j coefficient of ϵ in the $\mathcal{B}_1$ basis, $\epsilon = \sum_{j\in\mathcal{B}_1}[\epsilon]_j j$.

For a general CSS code family with the chain complex in Eq. (3), the X error-correction threshold is the largest p_c such that for all $p < p_c$ the probability of successful decoding goes to one in the limit of infinite system size

$$\mathrm{pr}(\mathrm{succ}) = \sum_{\epsilon\in C_1} \mathrm{pr}(\epsilon)\mathrm{pr}(\mathrm{succ}|\epsilon) \to 1. \quad (5)$$

With the optimal decoder, the conditional probability $\mathrm{pr}(\mathrm{succ}|\epsilon)$ equals one, if ϵ belongs to the most probable error equivalence class consistent with the syndrome $\partial_1\epsilon$, and zero otherwise. The probability of equivalence class $\bar{\epsilon}$ is

$$\mathrm{pr}(\bar{\epsilon}) = \sum_{\omega\in C_2} \mathrm{pr}(\epsilon+\partial_2\omega) \propto \sum_{\omega\in C_2} e^{-2\beta(p)\sum_{j\in\mathcal{B}_1}[\epsilon+\partial_2\omega]_j}, \quad (6)$$

where we use Eq. (4) and introduce

$$\beta(p) = -\frac{1}{2}\log\frac{p}{1-p}. \quad (7)$$

To rewrite Eq. (6), we use $[\partial_2\omega]_j \equiv \sum_{i\in\mathcal{B}_2\wedge\partial_2 i\ni j}[\omega]_i \bmod 2$ and $1-2[\epsilon+\partial_2\omega]_j = (-1)^{[\epsilon]_j+[\partial_2\omega]_j} = (-1)^{[\epsilon]_j}\prod_{i\in\mathcal{B}_2\wedge\partial_2 i\ni j}(-1)^{[\omega]_i}$. By introducing new (classical spin) variables $s_i = (-1)^{[\omega]_i}$ for all $i \in \mathcal{B}_2$, we can replace the sum over $\omega \in C_2$ in Eq. (6) by a sum over different configurations $\{s_i = \pm 1\}$, yielding

$$\mathrm{pr}(\bar{\epsilon}) \propto \sum_{\{s_i=\pm1\}} e^{-\beta(p)H_\epsilon(\{s_i\})}, \quad (8)$$

where we introduce the Hamiltonian

$$H_\epsilon(\{s_i\}) = -\sum_{j\in\mathcal{B}_1}(-1)^{[\epsilon]_j}\prod_{\substack{i\in\mathcal{B}_2\\ [\partial_2 i]_j=1}} s_i. \quad (9)$$

We define the random coupling Ising model to be a classical spin $s_i = \pm 1$ random model with quenched couplings $(-1)^{[\epsilon]_j}$ described by $H_\epsilon(\{s_i\})$ in Eq. (9). The RCIM has two independent parameters: disorder strength p (i.e., the probability of negative couplings) and inverse temperature β. The partition function of the RCIM with disorder ϵ at temperature β^{-1} is

$$Z_\epsilon(\beta) = \sum_{\{s_i=\pm1\}} e^{-\beta H_\epsilon(\{s_i\})}. \quad (10)$$

Note that for the proportionality $\mathrm{pr}(\bar{\epsilon}) \propto Z_\epsilon(\beta)$ to hold, one requires $\beta = \beta(p)$.

For the 3D color code, Eq. (9) leads to the following two new models

$$H^X_\epsilon(\{s_v\}) = -\sum_{t\in\Delta_3(\mathcal{L})}(-1)^{[\epsilon]_t} \quad (11)$$

$$H^Z_\epsilon(\{s_e\}) = -\sum_{t\in\Delta_3(\mathcal{L})}(-1)^{[\epsilon]_t} \quad (12)$$

relevant for X and Z error correction, respectively. Note that $H^X_\epsilon(\{s_v\})$ [respectively, $H^Z_\epsilon(\{s_e\})$] contains four-body (six-body) terms, which are products of vertex (edge) spins of every tetrahedron. We observe that, for $p = 0$, i.e., the case with no disorder, these two models are mutually dual in the sense that the low-temperature expansion of each model matches the high-temperature expansion of the other [35]; see the Supplemental Material [36].

The Hamiltonian in Eq. (9) determines a thermal ensemble of excitations in the statistical-mechanical model. For $H^X_\epsilon(\{s_v\})$, the excitations are 2D domain walls residing on a set of tetrahedra $\varphi = \epsilon + \partial_2\omega \in C_1$, where these walls terminate at the edges contained in $\partial_1\varphi = \partial_1\epsilon \in C_0$. In the color code, this ensemble of domain walls corresponds to the ensemble of possible X errors that generate the same syndrome as ϵ, and the Boltzmann weight of a wall configuration coincides with the probability of the corresponding X error configuration φ. Likewise, for $H^Z_\epsilon(\{s_e\})$, the excitations are 1D strings terminating at vertices in $\partial_1\epsilon$, corresponding to Z errors that generate the same error syndrome as ϵ.

To determine the storage threshold for the 3D color code, we investigate the disorder-temperature (p, T)-phase diagram of the RCIM in Eq. (9). In the ordered phase, large fluctuations of domain walls (or strings) are suppressed [3], and the free energy cost

$$\Delta_\lambda(\epsilon) = -\log Z_{\epsilon+\lambda}(\beta) + \log Z_\epsilon(\beta) \quad (13)$$

of introducing any nontrivial domain wall $\lambda \in \ker\partial_1\backslash\mathrm{im}\partial_2$ to the system at inverse temperature β with disorder ϵ should diverge in the limit of infinite system size when averaged over all disorder configurations,

$$\langle\Delta_\lambda\rangle = \sum_{\epsilon\in C_1}\mathrm{pr}(\epsilon)\Delta_\lambda(\epsilon) \to \infty. \quad (14)$$

Correspondingly, in the color code, the error φ produces a syndrome $\partial_1\varphi$ that points to a unique equivalence class $\bar{\varphi}$, so that the syndrome can be decoded successfully with high probability. Indeed, we show in the Supplemental Material, $\mathrm{pr}(\mathrm{succ}) \to 1$ for the error rate p implies $\langle\Delta_\lambda\rangle \to \infty$ for the RCIM at inverse temperature $\beta(p)$ and disorder strength p. Thus, by finding the critical point along the line defined by Eq. (7) (the Nishimori line [37]), we obtain the threshold value p_c.

Phase diagram.—We describe how to map out the (p, T)-phase diagrams of the two RCIMs, $H^X_\epsilon(\{s_v\})$ and $H^Z_\epsilon(\{s_e\})$. The discontinuity in energy density across a first-order phase transition allows for straightforward identification of the phase boundary in the regime of low disorder. However, more reliable order parameters are required to probe a (higher-order) phase transition close to the critical point on the Nishimori line. Moreover, an appropriate order parameter takes symmetries of the model into account. Note that flipping a subset of spins $\{s_i\}_{i\in I}$, i.e., $s_i \mapsto -s_i$ for $i \in I$, is a symmetry if it leaves the Hamiltonian describing the model invariant.

The four-body RCIM in Eq. (11) has a global $\mathbb{Z}_2 \times \mathbb{Z}_2 \times \mathbb{Z}_2$ symmetry. Flipping spins on all red and blue vertices is an example of a symmetry operation, since it leaves every term of $H^X_\epsilon(\{s_v\})$ unchanged. Because of this symmetry, the total magnetization is not a good order parameter. However, the sublattice magnetization of spins of a single color is a good parameter, as in the case of the spin model arising from the 2D color code [26,28]. Instead of using the sublattice magnetization directly, more precise estimations are obtained by considering the finite-size scaling of the spin-spin correlation function [38]. Near the phase transition, for fixed disorder strength p and temperatures T close to the critical temperature $T_c(p)$, the correlation length ξ_L is expected to scale as

$$\xi_L(p, T)/L \sim f(L^{1/\nu}[T - T_c(p)]), \tag{15}$$

where L is the linear system size, f is a scaling function, and ν is the correlation length critical exponent [39]. We estimate $T_c(p)$ by plotting $\xi_L(p, T)/L$ as a function of T for different L and finding their crossing point; see Figs. 3(a) and 3(b). If no crossing is observed, then we conclude that there is no phase transition.

The six-body RCIM in Eq. (12) describes a lattice gauge theory with a local $\mathbb{Z}_2 \times \mathbb{Z}_2$ symmetry. Flipping spins on edges from a single yellow vertex to all neighboring red and blue vertices is an example of a symmetry operation; see Fig. 2(c). Because of Elitzur's theorem [40], the gauge symmetry rules out existence of any local order parameter. We define a Wilson loop operator [41,42]

$$W(\gamma) = \prod_{e\in\gamma} s_e, \tag{16}$$

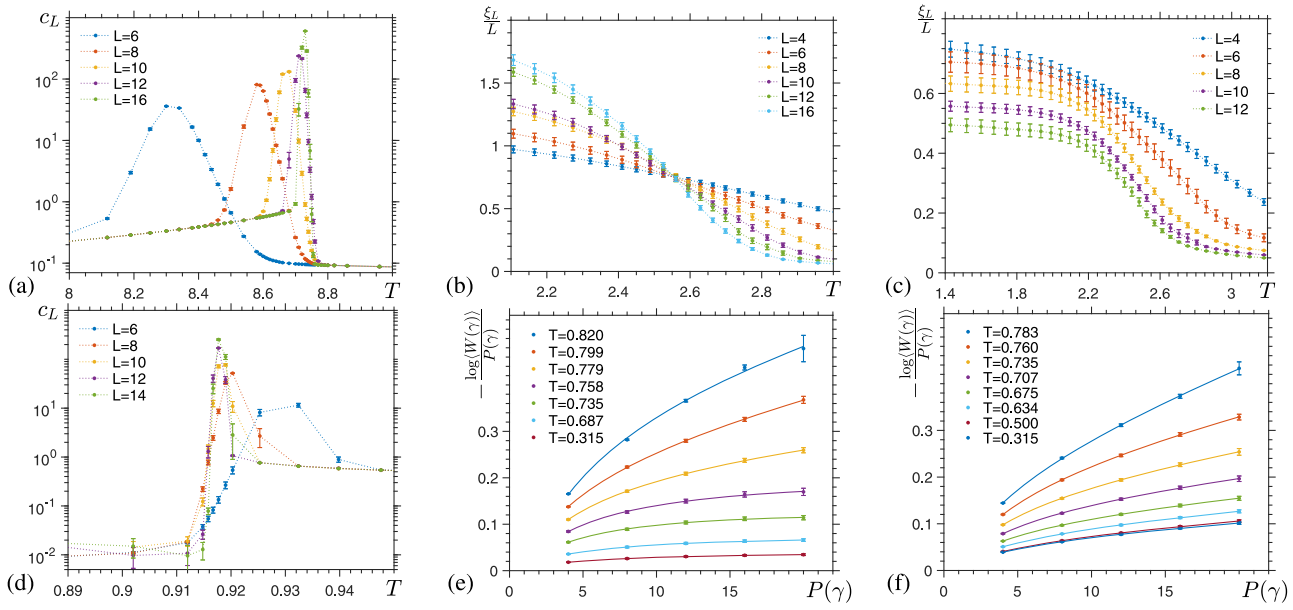

FIG. 3. Results for the 3D four body (a)–(c) and six-body (d)–(f) RCIMs. By finding peaks of specific heat c_L for different system sizes L and exploiting finite-size scaling, we estimate for $p = 0$ the critical temperature of a phase transition in (a) and (d) to be $T_c = 8.77(2)$ and $T_c = 0.918(3)$. (b) For $p = 0.27$, we identify $T_c = 2.56(4)$ as the intersection of normalized spin-spin correlation functions ξ_L/L for different L. (c) For $p = 0.28$, there is no indication of a phase transition. (e),(f) We check if the Wilson loop operator $W(\gamma)$ satisfies the perimeter law by plotting $-\log\langle W(\gamma)\rangle/P(\gamma)$ as a function of perimeter $P(\gamma)$ of the square loop γ for different T and $L = 10$. Solid lines show a numerical ansatz $aP(\gamma) + b + c\log P(\gamma)$ with fitting parameters a, b, c. The parameter a allows us to identify a phase transition; see the Supplemental Material [36]. (e) For $p = 0.018$, a change of scaling signalizes a phase transition at $T = 0.75(3)$, whereas (f) for $p = 0.021$, there is no indication that the system undergoes a phase transition.

to be a product of edge spins along a loop $\gamma \subset \Delta_1(\mathcal{L})$, similar to as in Ising lattice gauge theory [35]. For $W(\gamma)$ to be gauge invariant, the loop γ can only be composed of edges connecting vertices of two (out of four possible) colors. The phase transition is identified by analyzing scaling of the thermal expectation value of $W(\gamma)$ averaged over different disorder configurations

$$\langle W(\gamma)\rangle = \sum_{\epsilon \subset \Delta_3(\mathcal{L})} \mathrm{pr}(\epsilon) \sum_{\{s_e\}} W(\gamma) \frac{e^{-\beta H_\epsilon^Z(\{s_e\})}}{Z_\epsilon(\beta)}. \tag{17}$$

Namely, in the limit of large square loops [21,23,43], $-\log\langle W(\gamma)\rangle$ scales linearly with the loop's perimeter $P(\gamma)$ in the ordered (Higgs) phase, whereas in the disordered (confinement) phase, it scales linearly with the minimum area $A(\gamma)$ enclosed by γ; see Figs. 3(d)–3(f).

We find the (p, T)-phase diagrams of the four- and six-body RCIM by performing parallel tempering Monte Carlo simulations [29]; see Fig. 1. We test equilibration of the system by logarithmic binning of the data; we define the system to equilibrate when the last three bins agree within statistical uncertainty [26,28]. Since we simulate systems of finite size, a careful analysis of finite-size effects is necessary. Additional details are provided in the Supplemental Material [36], where we also study the related random plaquette Ising model to find an accurate estimate of the 3D toric code threshold $p^{(1)}_{\mathrm{3DTC}} \simeq 3.3\%$.

Discussion.—The 3D color code is a zero-rate code; thus, from the quantum Gilbert-Varshamov bound [44–46], we obtain the inequality $H(p^{(1)}_{\mathrm{3DCC}}) + H(p^{(2)}_{\mathrm{3DCC}}) \leq 1$ relating the phase- and bit-flip thresholds, where $H(p) = -p\log_2 p - (1-p)\log_2(1-p)$ is the Shannon entropy. Our numerical estimates $p^{(1)}_{\mathrm{3DCC}} \simeq 1.9\%$ and $p^{(2)}_{\mathrm{3DCC}} \simeq 27.6\%$ satisfy that constraint. In the Supplemental Material [36], which includes Refs. [47–52], we show how to heuristically estimate thresholds from the lattice parameters and compare with the analogous argument for the toric code.

The X stabilizers detecting Z errors are the same for the 3D stabilizer and subsystem color codes. Since the subsystem code has X and Z generators of identical support, its phase- and bit-flip thresholds for perfect measurements and optimal decoding are both equal to $p^{(1)}_{\mathrm{3DCC}}$. For the 3D color code on the bcc lattice, the threshold of the (efficient) projection decoder $p^{(1)}_{\mathrm{proj}} \simeq 0.75\%$ [18] is less than a half of $p^{(1)}_{\mathrm{3DCC}}$, justifying a search for better decoders.

We hope our Letter motivates further study of the 3D random coupling Ising models. We conjecture the existence of a spin-glass phase [53] in the six-body RCIM. A future extension of this work might incorporate measurement errors, which would require the study of 4D RCIMs and thus use more computational resources. If successful, this research program could provide a deeper understanding of single-shot error correction [14,15] from the standpoint of statistical mechanics.

We thank R. Andrist, H. Bombín, N. Delfosse, L. Pryadko, B. Yoshida, and I. Zintchenko for helpful discussions. A. K. would like to thank the QuArC group for their hospitality during a summer internship. We acknowledge funding provided by the Institute for Quantum Information and Matter, an NSF Physics Frontiers Center (NSF Grant No. PHY-1125565) with support of the Gordon and Betty Moore Foundation (GBMF-2644).

[1] A. Y. Kitaev, Ann. Phys. (Amsterdam) **303**, 2 (2003).
[2] S. B. Bravyi and A. Y. Kitaev, arXiv:9811052.
[3] E. Dennis, A. Kitaev, A. Landahl, and J. Preskill, J. Math. Phys. (N.Y.) **43**, 4452 (2002).
[4] S. Bravyi and A. Kitaev, Phys. Rev. A **71**, 022316 (2005).
[5] A. G. Fowler, M. Mariantoni, J. M. Martinis, and A. N. Cleland, Phys. Rev. A **86**, 032324 (2012).
[6] M. A. Levin and X.-G. Wen, Phys. Rev. B **71**, 045110 (2005).
[7] H. Bombin and M. A. Martin-Delgado, Phys. Rev. Lett. **97**, 180501 (2006).
[8] H. Bombin, in *Topological Codes*, edited by D. A. Lidar and T. A. Brun (Cambridge University Press, Cambridge, England, 2013).
[9] B. Zeng, A. Cross, and I. L. Chuang, IEEE Trans. Inf. Theory **57**, 6272 (2011).
[10] B. Eastin and E. Knill, Phys. Rev. Lett. **102**, 110502 (2009).
[11] H. Bombin and M. A. Martin-Delgado, Phys. Rev. B **75**, 075103 (2007).
[12] H. Bombin, New J. Phys. **17**, 083002 (2015).
[13] A. Kubica, B. Yoshida, and F. Pastawski, New J. Phys. **17**, 083026 (2015).
[14] H. Bombín, Phys. Rev. X **5**, 031043 (2015).
[15] B. J. Brown, N. H. Nickerson, and D. E. Browne, Nat. Commun. **7**, 12302 (2015).
[16] A. Kubica and M. E. Beverland, Phys. Rev. A **91**, 032330 (2015).
[17] N. Delfosse, Phys. Rev. A **89**, 012317 (2014).
[18] A. Kubica, Ph.D. thesis, California Institute of Technology, 2017.
[19] Y. Ozeki and N. Ito, J. Phys. A **31**, 5451 (1998).
[20] M. Hasenbusch, F. Parisen Toldin, A. Pelissetto, and E. Vicari, Phys. Rev. B **76**, 184202 (2007).
[21] T. Ohno, G. Arakawa, I. Ichinose, and T. Matsui, Nucl. Phys. **B697**, 462 (2004).
[22] A. Honecker, M. Picco, and P. Pujol, Phys. Rev. Lett. **87**, 047201 (2001).
[23] C. Wang, J. Harrington, and J. Preskill, Ann. Phys. (Amsterdam) **303**, 31 (2003).
[24] A. A. Kovalev and L. P. Pryadko, Quantum Inf. Comput. **15**, 825 (2015).
[25] I. Dumer, A. A. Kovalev, and L. P. Pryadko, Phys. Rev. Lett. **115**, 050502 (2015).
[26] H. G. Katzgraber, H. Bombin, and M. A. Martin-Delgado, Phys. Rev. Lett. **103**, 090501 (2009).
[27] H. Bombin, R. S. Andrist, M. Ohzeki, H. G. Katzgraber, and M. A. Martin-Delgado, Phys. Rev. X **2**, 021004 (2012).
[28] R. S. Andrist, Ph.D. thesis, ETH Zurich, 2012.

[29] K. Hukushima and K. Nemoto, J. Phys. Soc. Jpn. **65**, 1604 (1996).
[30] The 3D subsystem color code has the gauge group $\mathcal{G} = \langle \prod_{\Delta_3(\mathcal{L})\ni t\supset e} X(t), \prod_{\Delta_3(\mathcal{L})\ni t\supset e} Z(t) | e \in \Delta_1(\mathcal{L})\rangle$ and the stabilizer group $\mathcal{S} = \langle \prod_{\Delta_3(\mathcal{L})\ni t\supset v} X(t), \prod_{\Delta_3(\mathcal{L})\ni t\supset v} Z(t) | v \in \Delta_0(\mathcal{L})\rangle$.
[31] D. Gottesman, Phys. Rev. A **54**, 1862 (1996).
[32] A. R. Calderbank, E. M. Rains, P. W. Shor, and N. J. A. Sloane, Phys. Rev. Lett. **78**, 405 (1997).
[33] For correction of Z errors, exchange $X \leftrightarrow Z$ and redefine $\mathcal{B}_2 = \Delta_1(\mathcal{L})$, $\mathcal{B}_1 = \Delta_3(\mathcal{L})$, $\mathcal{B}_0 = \Delta_0(\mathcal{L})$, $\partial_2 e = \sum_{\Delta_3(\mathcal{L})\ni t\supset e} t$, and $\partial_1 t = \sum_{\Delta_0(\mathcal{L})\ni v\subset t} v$ for any $e \in \Delta_1(\mathcal{L})$ and $t \in \Delta_3(\mathcal{L})$.
[34] M. H. Freedman and D. A. Meyer, Found. Comput. Math. **1**, 325 (2001).
[35] F. J. Wegner, J. Math. Phys. (N.Y.) **12**, 2259 (1971).
[36] See Supplemental Material at http://link.aps.org/supplemental/10.1103/PhysRevLett.120.180501 for heuristic estimates of thresholds, the duality of spin models, the proof of the implication, additional results on the random plaquette Ising model and numerical simulation details.
[37] H. Nishimori, Prog. Theor. Phys. **66**, 1169 (1981).
[38] M. Palassini and S. Caracciolo, Phys. Rev. Lett. **82**, 5128 (1999).
[39] N. Goldenfeld, *Lectures on Phase Transitions and Critical Phenomena* (Addison-Wesley, Reading, MA, 1992).
[40] S. Elitzur, Phys. Rev. D **12**, 3978 (1975).
[41] K. G. Wilson, Phys. Rev. D **10**, 2445 (1974).
[42] J. Kogut, Rev. Mod. Phys. **51**, 659 (1979).
[43] M. Creutz, L. Jacobs, and C. Rebbi, Phys. Rev. D **20**, 1915 (1979).
[44] E. N. Gilbert, Bell Syst. Tech. J. **31**, 504 (1952).
[45] R. Varshamov, Sov. Phys. Dokl. **117**, 739 (1957).
[46] A. R. Calderbank and P. W. Shor, Phys. Rev. A **54**, 1098 (1996).
[47] M. Kardar, *Statistical Physics of Fields* (Cambridge University Press, Cambridge, England, 2007).
[48] M. S. S. Challa, D. P. Landau, and K. Binder, Phys. Rev. B **34**, 1841 (1986).
[49] K. Binder, Rep. Prog. Phys. **50**, 783 (1987).
[50] J. Lee and J. M. Kosterlitz, Phys. Rev. B **43**, 3265 (1991).
[51] C. Borgs and R. Kotecky, Phys. Rev. Lett. **68**, 1734 (1992).
[52] H. G. Katzgraber, S. Trebst, D. A. Huse, and M. Troyer, J. Stat. Mech. (**2006**) P03018.
[53] K. Binder and A. P. Young, Rev. Mod. Phys. **58**, 801 (1986).